OBSERVATIONS OF FLUXES OVER HETEROGENEOUS SURFACES

L. MAHRT

Oceanic and Atmospheric Sciences, Oregon State University, Corvallis, OR, 97331, USA

J. I. MACPHERSON

Flight Research Laboratory, National Research Council, Ottawa, ON, K1A OR6, Canada

and

RAY DESJARDINS

Centre for Land and Biological Resource Research, Agriculture Canada, Ottawa, ON, K1A 006, Canada

(Received in final form 25 May, 1993)

Abstract. This study analyzes data collected from repeated aircraft runs 30 m over alternating regions of irrigated and dry nonirrigated surfaces, each region on the order of 10 km across, during the California Ozone Deposition Experiment (CODE). After studying the scale dependence of the flow, the variables and their fluxes are decomposed into means for sublegs defined in terms of irrigated and nonirrigated regions and deviations from such subleg means. Since the repeated runs were flown over the same track, compositing the eight flight legs for each of the two days allows partial isolation of the influences of surface heterogeneity and transient mesoscale motions.

A variance analysis is carried out to quantify the relative importance of surface heterogeneity and transient mesoscale motions on the variability of the turbulence fluxes. The momentum and ozone fluxes are more influenced by transient mesoscale motions while fluxes of heat, moisture and carbon dioxide are more influenced by surface heterogeneity. The momentum field is also influenced by a quasi-stationary mesoscale front and larger scale velocity gradients.

For the present case, the mesoscale modulation of the turbulent flux is numerically more important than the direct mesoscale flux. This spatial modulation of the turbulent fluxes leads to extra Reynolds terms which act to reduce the area-averaged turbulent momentum flux and enhance the area-averaged turbulent heat flux.

1. Introduction

Surface variability affects the relationship between spatially averaged fluxes and spatially averaged vertical gradients (Claussen, 1991). Spatial averaging is implied over each subgrid area in numerical models of boundary-layer flow. Smith *et al.* (1992) demonstrate some of the difficulties of forming spatially averaged fluxes from a surface network even over relatively homogeneous surfaces. In general, it is not possible to construct a sufficiently dense measurement network to observe each field or surface feature (Desjardins *et al.*, 1992). While it is unlikely that an accurate and practical formulation of fluxes over heterogeneous surfaces can be constructed, it may be possible to improve upon existing formulations which are based on homogeneous flow. However, it is first necessary to further study the

Boundary-Layer Meteorology **67**: 345–367, 1994.

behavior of fluxes over heterogeneous surfaces. The goal of this study is to examine the relationship between low level fluxes and spatial variability of surface moisture and vegetation. This study analyzes fluxes over areas of systematically irrigated croplands and areas of dry grassland or bare soil. Each area is on the order of 5–15 km across. This flow situation falls into the "organized" case discussed in André *et al.* (1989) and is compatible with subdividing grid areas into distinct subgrid surface types as in the modelling philosophy of Avissar and Pielke (1989), Ducoudré *et al.* (1993) and Huang and Lyons (1993). The well defined surface conditions in this study contrast to the case of random small-scale variability described by "statistical heterogeneity" (Mason, 1988); in this case, the flow higher in the boundary layer, above the "blending height", may achieve collective equilibrium with the various surface types and therefore not vary significantly within the grid area at that level.

2. The Data and Scale Dependence

This study analyzes data from the California Ozone Deposition Experiment (CODE) consisting of eight, 33 km legs flown at 30 m above the terrain over the same track on both 23 July 1991 (Flight 13) and 30 July 1991 (Flight 19). The instrumentation is described in MacPherson (1992) and MacPherson *et al.* (1993). Both days are characterized by clear skies. Winds are from the northwest at about 5 m/s during flight 13 and light with variable wind direction during flight 19. The eight legs for flight 13 were executed approximately between 1300–1500 local solar time, while the eight flight legs for flight 19 were carried out approximately between 1045–1245 local solar time. Flight 19 contains a little more diurnal evolution. This study will emphasize flight 13 and report results for flight 19 only when they are significantly different from those of flight 13.

The surface heterogeneity is well defined by the greenness index (Figure 1), which is the ratio of near infrared radiation centered at 0.73 μ to the infrared radiation centered at 0.66 μ. The surface radiation temperature varies by about 20 °C between the irrigated croplands and nonirrigated areas similar to the variation in Doran *et al.* (1992) and about twice that in Segal *et al.* (1989). The heterogeneity in this study is considerably stronger than that in Hechtel *et al.* (1990) where typical variations of surface temperature of 1 °C over 1 km or less produced little observable impact on the boundary layer. The air temperature at 30 m in this study varies by 1.0–1.5 °C between irrigated and nonirrigated areas (Figure 1). Although the surface temperature variations are weaker in Segal *et al.* (1989), they occur on a larger scale and produce air temperature differences as large as in the present study.

We attempt to identify the scale of the main transporting eddies as well as any scales imposed by the surface heterogeneity. As tools for display of the scale dependence, we have computed the Fourier and the non-orthogonal Haar spectra (Mahrt, 1991a; Gamage and Hagelberg, 1993). The Haar spectrum is based on a

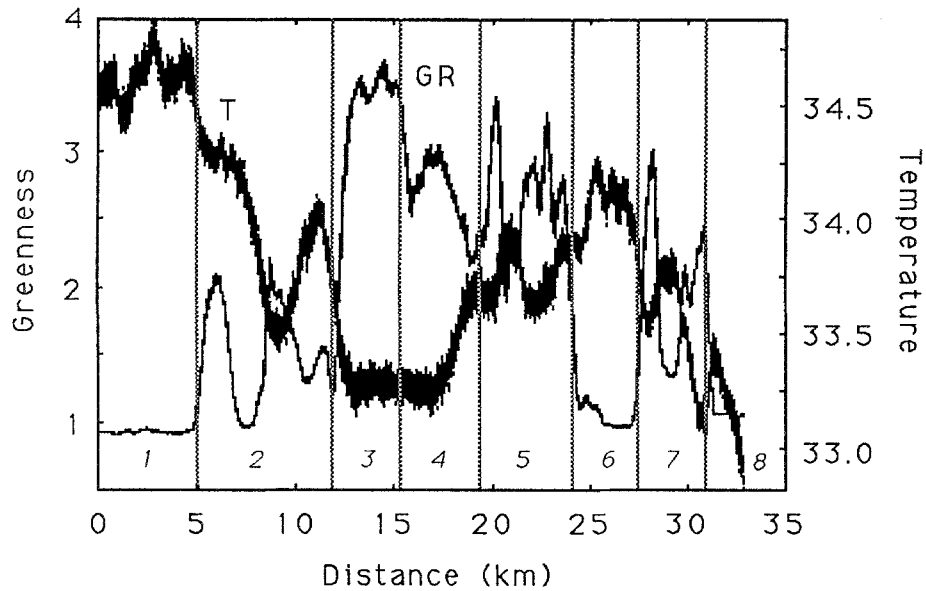

Fig. 1. Greenness index and air temperature defined as a moving average with a window width of 375 m and composited over all flight legs for Flight 13, defined as $\{\phi^*(x, t)\}$ in Section 3a. Northeast (southwest) is directed to the right (left). Vertical lines indicate partitioning of the flight legs into sublegs, defined in Section 3b.

local step function as a basis function defined over different scales (dilations), as opposed to the Fourier spectrum which is based on sines and cosines at different wavelengths. The Haar transform is defined independently for different positions within the record (translations) as opposed to the Fourier transform which is global and generates one complex coefficient for the entire record. The Haar spectrum is computed by summing the square of the transform coefficients over the different positions in the record for a given scale and then repeating this sum for each scale to form the energy dependence on scale. The present study employs nonorthogonal spectra to better isolate the spectral peaks (Mahrt, 1991a) although orthogonal spectra can be extracted *a posteriori*. For conditions of relatively stationary homogeneous flow, the spectral peaks based on the Haar transform occur at scales which are generally two or three times smaller than the Fourier spectrum. The Haar spectral peak measures the width of the main structures while the Fourier spectral peak measures the scale of principal periodicity which includes the spacing between the structures. For the present data, the Fourier spectra are noisier and less amenable to detecting peaks compared to the Haar spectra but generally show peaks at roughly twice the scale of the peak of the Haar spectra. Irregularly spaced sharp transitions associated with field boundaries contribute to the noise in the Fourier spectra. For brevity, we show only the Haar spectrum.

The Haar spectrum for vertical velocity shows a well defined peak at about

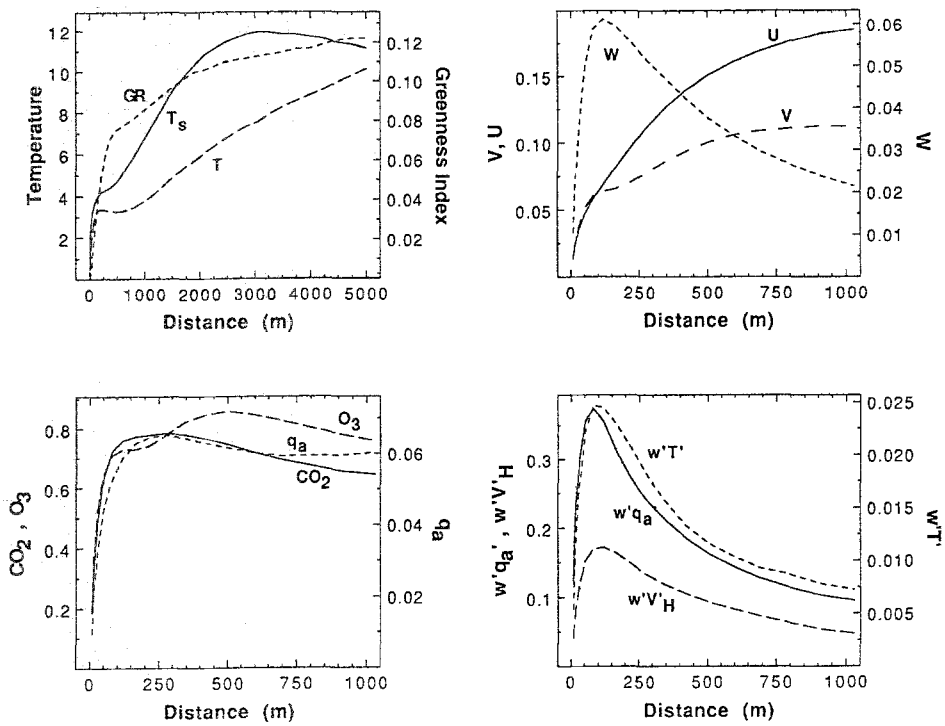

Fig. 2a.

125 m (Figure 2a) while moisture and carbon dioxide show broader peaks. The other variables tend to show at least a relative peak at scales of a few hundred meters or less but also show considerable variance at larger scales. The mesoscale peak associated with the surface heterogeneity is well defined only for the surface temperature which shows maximum variance at about 3–3½ km while the peak for the greenness index exhibits flattening beginning at about 5 km (Figure 2a). We cannot study scales much larger than 5 km with statistical reliability because the record lengths are only 33 km. The peaks are relatively broad due to the variable size of the irrigated and nonirrigated areas and substructure within each area.

The Haar spectra for the vertical fluxes[1] generally show a maximum around 100 m corresponding to the peak for vertical velocity. The Fourier cospectra generally show maxima at scales of a few hundred meters with significant flux extending to near 1 km and countergradient momentum flux at wavelengths larger than 1 km.

[1] Here the Haar spectrum for the fluxes is computed by considering the flux to be just another variable in which case the spectra are a measure of the scale dependence of the flux variance. In this sense, the Haar spectrum presented here are not analogous to the Fourier cospectrum.

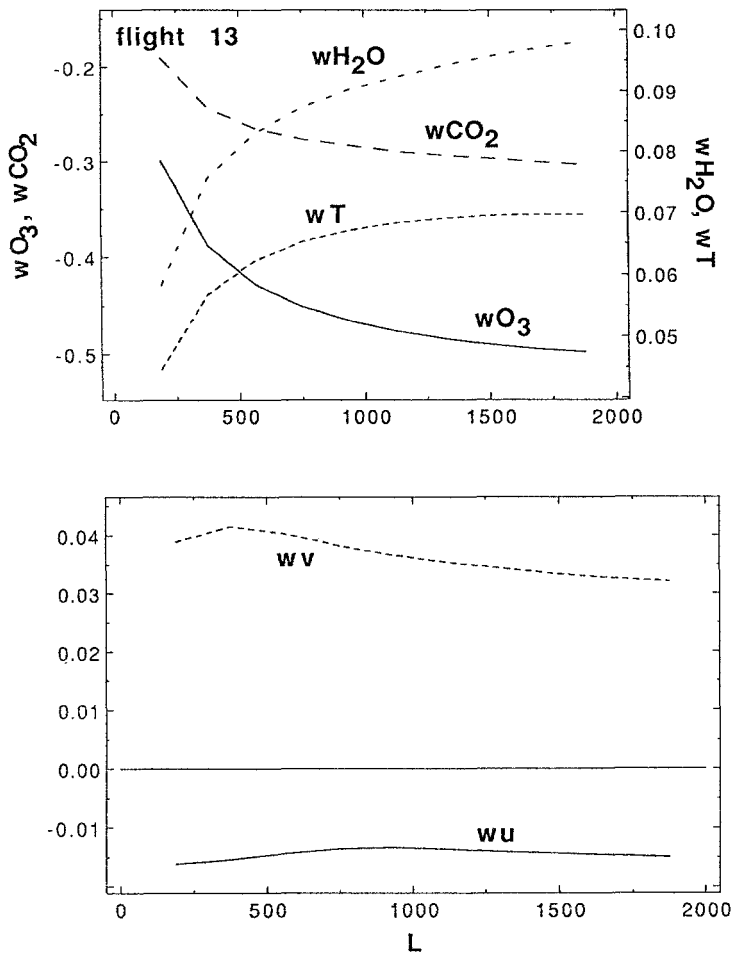

Fig. 2. a) Non-orthogonal Haar spectra for the greenness index, surface temperature (T_s, $°K^2$), air temperature (T, $°K^2$), the three velocity components ($m^2 s^{-2}$), specific humidity ($g^2 Kg^{-2}$), carbon dioxide ($mg^2 Kg^{-2}$), ozone (ppb^2), and the variance spectra for turbulent flux of momentum ($m^4 s^{-4}$), heat ($m^2 s^{-2} °K^2$), specific humidity ($m^2 s^{-2} g^2 Kg^{-2}$), carbon dioxide ($m^2 s^{-2} mg^2 Kg^{-2}$) and ozone from the DLR ozone analyzer ($m^2 s^{-2} ppb^2$) for flight 13. b) Scale dependence of the turbulent fluxes computed as the deviations from a moving average for varying window width for flight 13.

In subsequent sections, we shall analyze fluxes computed from fluctuations from a moving average. These fluxes, averaged over the record length, are plotted as a function of window width in Figure 2b. This momentum flux reaches a maximum at a window width of about 375 m implying countergradient fluxes at scales larger than 375 m. Within the ability of the aircraft soundings to define the vertical gradients, the countergradient momentum fluxes do not appear to be related to a reversal of vertical gradients of wind components with height. The unique behavior

of the turbulent momentum flux appears to be partly related to transient mesoscale circulations as will be discussed in subsequent sections.

We conclude that the scale of maximum flux is determined by the scale of maximum vertical velocity variance and that this scale is a few hundred meters or less depending on the computational method. Figure 2b indicates that most of the flux can be captured with a window width of 500 m. However a budget study requiring a quantitative estimate of the total flux would be better served by a much wider window width.

To study the spatial variability of the fluxes in Section 3a and Sections 6–7, we shall choose a window width of 375 m. Although this excludes some of the flux, it also eliminates the countergradient momentum flux and minimizes smoothing of the transitions between irrigated and nonirrigated areas. For more quantitative analysis in Section 3b, Section 4 and briefly in Sections 6–7, we shall partition the record into natural segments of roughly 5 km, based on the greenness index, and compute the fluxes in terms of deviations of subleg averages.

3. Partitioning Mesoscale and Turbulence Motions

A. Partitioning

The analysis of scale dependence in the preceding section indicated considerable variance on scales of 5 km and greater which we shall arbitrarily refer to as mesoscale variations. Large mesoscale motions are not fully included in these data since the flight legs are only 33 km long. Part of the mesoscale variability is associated with surface heterogeneity and part is associated with transient mesoscale motions.

We define a local average $[\phi(x,t)]$ and partition the local average in terms of the spatial average along the entire aircraft leg $\langle\phi(x,t)\rangle$ and deviations from this spatial average $\phi^*(x,t)$ so that

$$[\phi(x,t)] = \langle\phi(x,t)\rangle + \phi^*(x,t)\,, \tag{1}$$

where x is the distance along the aircraft leg and $\phi(x,t)$ represents one of the velocity components, temperature, moisture or one of the chemical species. The local average $[\phi(x,t)]$ will be defined as either a local running mean or a simple average over sublegs corresponding to regions of irrigated or nonirrigated surfaces (Figure 1).

Using (1), the total flow is then decomposed as

$$\phi(x,t) = [\phi(x,t)] + \phi'(x,t) = \langle\phi(x,t)\rangle + \phi^*(x,t) + \phi'(x,t)\,, \tag{2}$$

where $\phi'(x,t)$ is the turbulent part of the signal computed as deviations from $[\phi(x,t)]$.

There are many different methods of constructing the partitioning (2) from actual data. The partitioning between the mesoscale flow $\phi^*(x,t)$ and turbulent

fluctuations $\phi'(x, t)$ will be defined in two different ways. In the first approach, a local mean $[\phi(x, t)]$ is defined as a moving average with a window width of 375 m. This approach will be used to construct an impression of spatial variability of the turbulent fluxes but $[\phi(x, t)]$ is defined on a scale too small to serve as a partition between turbulence and mesoscale motions. The second approach uses surface-based partitioning on a scale of about 5 km and will provide a better partitioning between turbulence and mesoscales. Results from the two approaches will be compared since no mathematical partitioning is physically unambiguous.

To estimate the contributions of the surface heterogeneity, we reduce the influence of transient mesoscale motions by compositing $[\phi(x, t)]$ over all eight aircraft legs to obtain $\{[\phi(x, t)]\}$, where the operator $\{\}$ indicates an average over all of the flight legs at a given location x. Therefore $\{[\phi(x, t)]\}$ is an estimate of the stationary part of the spatial variation but also contains significant transient fluctuations which are not completely removed by the compositing (Figure 3). The moving average is sequentially translated only one point at a time (approximately 3.5 m) so that $\{[\phi(x, t)]\}$ includes sharp transitions associated with surface variability; unfortunately, this procedure also includes more of the influence of small-scale turbulence fluctuations. The estimate of the stationary part of the turbulent fluxes is computed by compositing $w'\phi'$ over the 8 flight legs to obtain $\{w'\phi'\}$ for each location. Since $w'\phi'$ is not smoothed before compositing, it also includes significant small-scale variations which were only partially removed by the compositing.

The composited results are shown in Figure 1 and Figures 3–4. The estimate of the stationary spatial variation of air temperature, $\{[T(x, t)]\}$, is strongly related to the surface heterogeneity with expected cooler air temperatures over the irrigated areas, particularly in the central part of the observational domain (Figure 1) where again the areas of irrigated vegetation are indicated by the large greenness index. The estimated stationary part of the flow shows a modest tendency for greater moisture and less carbon dioxide and ozone over the irrigated areas in the central part of the flight region (Figure 3) probably due to transpiration and plant uptake of carbon dioxide and ozone.

The estimated stationary part of the v-component, $\{[v(x, t)]\}$, indicates a weak tendency for weaker momentum over irrigated areas. The latter is due to weaker instability over irrigated areas and resulting smaller downward mixing of horizontal momentum (Figure 4). This leads to a dramatic shear zone at the eastern edge of the irrigated region at the boundary between sublegs 5 and 6.

The composited turbulent flux $\{[w'\phi']\}$ of heat, and sometimes of moisture and carbon dioxide, (Figure 4) show sharp changes at boundaries between irrigated and nonirrigated fields. The fluxes of momentum and sometimes ozone show a rather obscure relation to the variations of the greenness index. The sharp transitions in the spatial variation of the heat flux might be enhanced by local advection. Advection of cool air from irrigated fields to the dry fields increases the upward heat flux. Advection of warm air from dry fields to the vegetated fields leads to

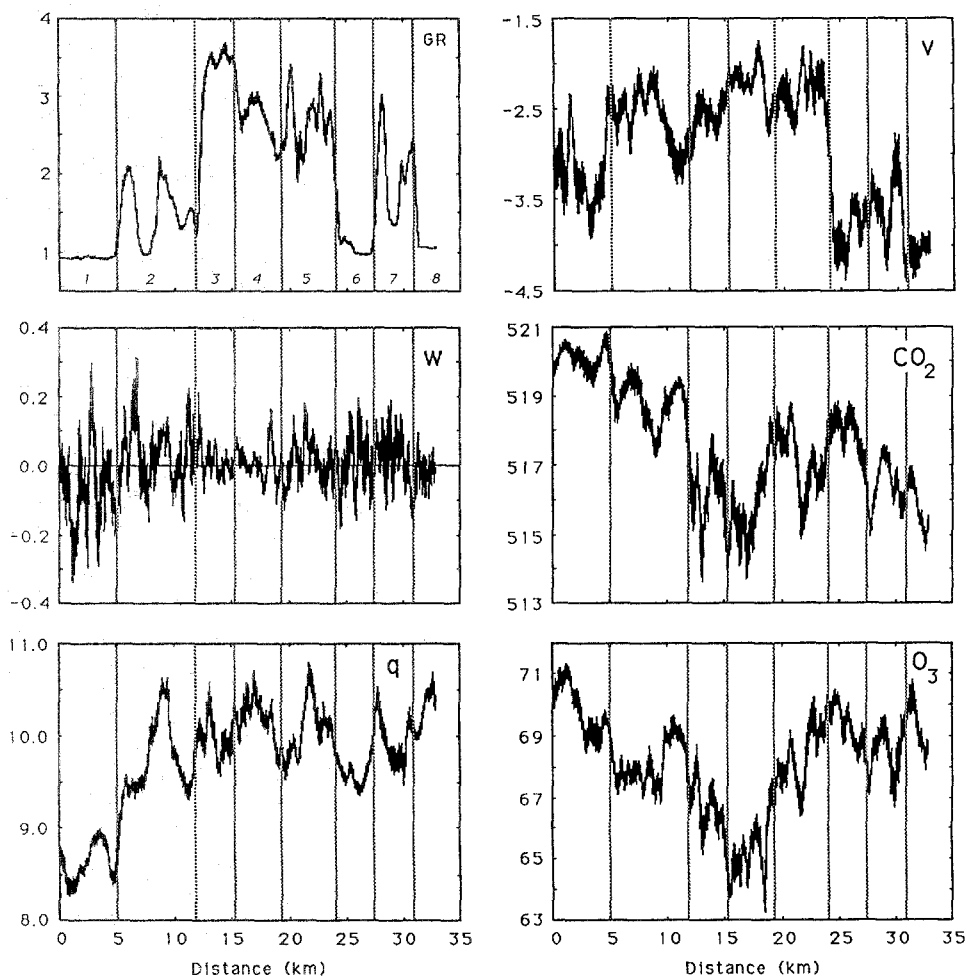

Fig. 3. Spatial variation defined as a moving average translated one point at a time (approximately 3.5 m) with a window width of 375 m and composited over all of the flight legs for Flight 13 defined as $[\phi(x, t)]$ in Section 3a for the v and w velocity components ($m^1 s^{-1}$), specific humidity ($g^1 Kg^{-1}$), carbon dioxide ($mg\,Kg^{-1}$) and ozone (ppb).

weak downward heat flux, also observed in Bache and Unsworth (1977), Lange *et al.* (1983), and de Bruin *et al.* (1991). Over the CODE domain, the buoyancy flux (virtual heat flux) is still upward over all of the irrigated areas, even if weak, so that the flow is everywhere unstably stratified. As possible examples of the influence of advection, the strongest heat flux over subleg six and over the dry fields within subleg two occur at the upstream (eastern) edges, as is also implied in the observational study of Vugts and Businger (1977) and others. At the upstream edge, cold air advection enhances the surface-atmosphere temperature difference.

The transition between irrigated and nonirrigated areas, as observed from the

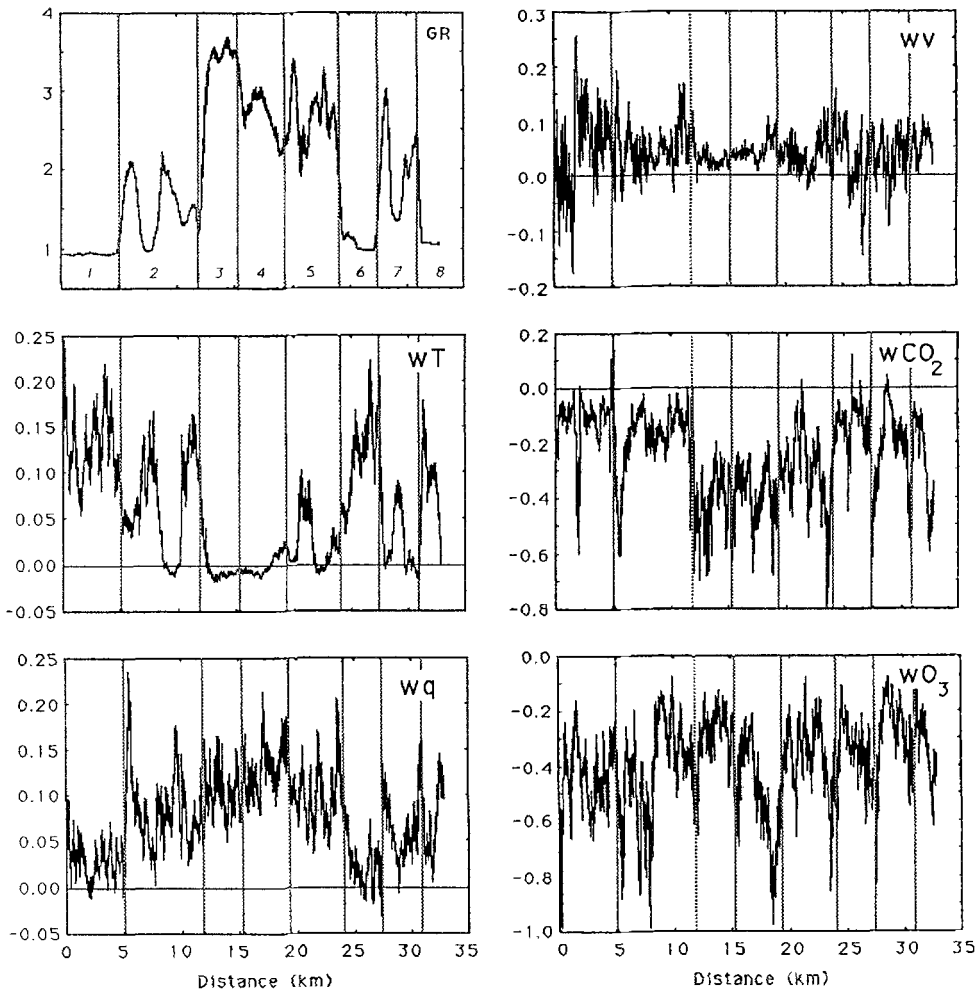

Fig. 4. Spatial variation of instantaneous turbulent fluxes defined from deviations from a moving average with a window width of 375 m and composited over all of the flight legs ($\{w'\phi'\}$, Section 3a) for Flight 13 for the fluxes of v-momentum ($m^2 s^{-2}$), heat (ms^{-1} deg. K), specific humidity ($m\,s^{-1}\,g\,Kg^{-1}$), carbon dioxide ($m\,s^{-1}\,mg\,Kg^{-1}$) and ozone ($m\,s^{-1}$ ppb).

heat flux and other variables at the 30 m level, often seems to occur almost directly above the discontinuity of the greenness index. This is apparently due to the fact that the thermal rise rate is as strong as the east-west (cross-field) component of the wind. However, the data seem inadequate to pose a formal comparison with internal boundary-layer models such as surveyed in Garratt (1990, 1992)

B. Variance analysis using surface-based partitioning

To quantitatively estimate the importance of the surface heterogeneity, we construct a variance analysis from the decomposition (1) as is schematically illustrated

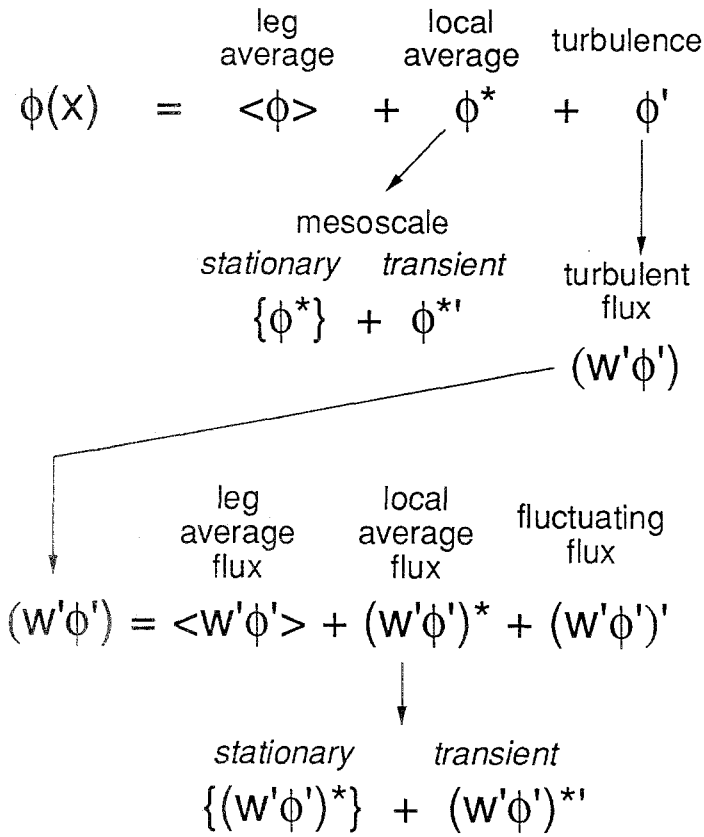

Fig. 5. A schematic flow chart of the flow decomposition.

in Figure 5. To emphasize the influence of surface heterogeneity, we partition the flight legs into eight sublegs determined from spatial variations of the greenness index and compute $[\phi(x, t)]$ to be the subleg average. The subleg boundaries are located in Figure 1. The record for each flight leg is translated and sometimes slightly "stretched" in order that the sharp changes of the greenness index occur at the same relative position for each of the flight legs. The spatial variation of the radiative surface temperature agrees closely with the spatial variation of the greenness index and would have led to approximately the same subleg boundaries. The sublegs are characterized by predominantly green irrigated cropland (sublegs 3–5), dry grassland and or bare fields (subleg 1, 6 and 8) or a mixture (sublegs 2 and 7).

Turbulent fluctuations are then mathematically defined as the deviations from the subleg average. For simplicity, we remove the global mean $\{\langle[\phi(x, t)]\rangle\}$ from all the variables where again $\langle\,\rangle$ represents averaging over a given aircraft leg and $\{\}$ averages variables over all of the aircraft legs. Since we apply simple unweighted

averaging, the cross-terms vanish and the variance decomposition based on (1) composited over all of the flight legs becomes simply

$$\{\langle[\phi(x,t)]^2\rangle\} = \{\langle\phi(x,t)\rangle^2\} + \{\langle\phi(x,t)^{*2}\rangle\} . \tag{3}$$

The first term on the right hand side $\{\langle\phi(x,t)\rangle^2\}$ is the variance due to the temporal variation of the variables between the flight legs and is due mainly to diurnal trend. The second term is the "mesoscale" variance due to spatial variation along the flight track, where again $\phi(x,t)^*$ is the deviation of the local average from the flight leg mean.

We further decompose $\phi(x,t)^*$ into a stationary part which has been "time" averaged over all of the flight legs $\{\phi(x,t)^*\}$ and a deviation from this time average $\phi(x,t)^{*\prime}$ so that

$$\phi(x,t)^* = \{\phi(x,t)^*\} + \phi(x,t)^{*\prime} . \tag{4}$$

Then the variance decomposition (3) becomes

$$\{\langle[\phi(x,t]\rangle^2\rangle\} = \{\langle\phi(x,t)\rangle^2\} + \langle\{\phi(x,t)^*\}^2\rangle + \{\langle\phi(x,t)^{*\prime 2}\rangle\} . \tag{5}$$

The second term on the right hand side is the variance due to the time averaged spatial structure which we shall refer to as the "stationary spatial variation". For most of the variables, the stationary spatial structure represents primarily the influence of the surface heterogeneity. The last term represents mainly the variance due to the transient deviations from the time averaged flow and will be referred to as the "transient mesoscale variance". The variance analysis (5) is now applied to the subleg averages of the variables and the subleg averages of the turbulent fluxes.

We first apply the decomposition of total variance (5) to the fluxes; that is, the decomposed variable $\phi(x,t)$ in (5) is now replaced with the subleg turbulent flux of $\phi(x,t)$ as schematically illustrated in the lower part of Figure 5. More than 80% of the total variance of the heat flux is described by the spatial variation associated with the surface heterogeneity (Table I). About half of the variance of the moisture and carbon dioxide flux is explained by the surface heterogeneity while only about 20% of the ozone and momentum flux is related to the surface heterogeneity. More than half of the variance of the momentum and ozone fluxes is associated with transient mesoscale variations. The transient behavior of the momentum flux can be tentatively related to transient pressure perturbations; the failure of the ozone flux to respond to the surface variations will be examined in a subsequent investigation.

The variance of temperature is controlled by both the surface heterogeneity and the temporal variation associated with diurnal trend (Table I). After removing the diurnal trend, the variation between the irrigated and nonirrigated land completely dominates the temperature variation. The moisture variance is dominated by the surface heterogeneity with negligible diurnal trend. The importance of the spatial variation of horizontal momentum (Table I) appears to be due partly to the large-

TABLE I

Variance decomposition for flights 13 and 19 (parenthesis) scaled by total variance. The columns are, respectively, the three terms on the right hand side of (5) which are the temporal variation on the spatially averaged flow, the stationary spatial variance, and the remaining transient deviations.

	Temporal	Spatial	Transient
u	0.32 (012)	0.57 (0.78)	0.11 (0.10)
v	0.31 (0.13)	0.57 (0.80)	0.12 (0.07)
w	0.09 (0.08)	0.06 (0.20)	0.85 (0.72)
θ	0.37 (0.50)	0.61 (0.48)	0.02 (0.02)
q	0.01 (0.09)	0.81 (0.81)	0.18 (0.10)
CO_2	0.40 (0.86)	0.51 (0.11)	0.09 (0.03)
O_3	0.16 (0.27)	0.57 (0.34)	0.27 (0.39)
T_{sfc}	0.01 (0.01)	0.99 (0.99)	0.00 (0.00)
$[w'u']$	0.14 (0.06)	0.28 (0.17)	0.58 (0.77)
$[w'v']$	0.07 (0.03)	0.24 (0.11)	0.69 (0.86)
$[w'\theta']$	0.03 (0.02)	0.89 (0.82)	0.08 (0.16)
$[w'q']$	0.12 (0.07)	0.46 (0.51)	0.42 (0.42)
$[w'CO_2']$	0.09 (0.02)	0.56 (0.57)	0.35 (0.41)
$[w'O_3']$	0.14 (0.09)	0.17 (0.23)	0.69 (0.68)

scale spatial trend discussed in Section 2. These influences lead to relatively low correlation between the horizontal wind and the greenness index. The weak relation between the low level wind field and the spatial variations of surface wetness is also evident in Figure 7 of Pielke and Avissar (1990).

In contrast to the other variables, vertical motion is mainly controlled by transient mesoscale variations (Table I). This may explain why mesoscale fluxes for most of the variables are erratic and small when averaged over all flight legs. In other terms, the variation of surface heating fails to generate a well defined thermal circulation. The lack of organized mesoscale vertical motion may be due to the fact that the irrigated and nonirrigated areas are only about 10 km across and may also be due to the relatively low level (30 m) of the flight legs. Segal *et al.* (1989) suggest that surface features must be organized on a scale greater than 20–30 km in order to generate convectively driven circulations, depending on the strength of the larger scale flow. The linear analysis of Smith and Mahrt (1981) indicates that motions driven by smaller scale variations of surface heat flux are damped by pressure adjustments. These pressure adjustments are induced by vertical motions in the presence of stable stratification, here associated with the subsidence inversion and stratification of the overlying flow. The numerical study of Hadfield *et al.* (1992) also indicates that circulations generated by differential surface heating increase with the scale of the surface variation and decrease substantially with specification of even a small mean wind speed. Perhaps the tilting of warm and cool cores by the mean wind leads to thermal interference in terms of the associated hydrostatic pressure variations at the surface. The minimum size of heated and

cooled regions required to generate mesoscales circulations is discussed further in Segal and Arritt (1992).

The temporal variances for temperature, moisture and the chemical species are generally more important for flight 19 due to the capture of the greater diurnal variation of late morning. Additionally, the spatial variation of the horizontal velocity field is more important for flight 19. Except for these differences, the two days show similar variance budgets.

Time-distance cross-sections for the transient mesoscale fields ($\phi(x, t)^{*\prime}$) for the wind components and ozone seem to be organized into coherent circulations with a horizontal "wavelength" (projected onto the flight path) of about 25 km with a phase propagation speed (projected onto the flight path) of about 5 m/s toward the southwest. These circulations also significantly affect the spatial distribution of moisture and to a lesser extent the distribution of carbon dioxide. The transient circulations exert only a weak influence on the temperature distribution which is consistent with the small contribution of the transient part of the variance budget for both temperature and heat flux (Table I). Although the transient mesoscale structure does not have a large amplitude, its coherent spatial structure organizes the instantaneous spatial distribution of the turbulent moisture flux. Mahrt (1991b) also observed significant organization of the moisture field by transient mesoscale motions with only weak variation of the temperature and vertical motion fields. It may be that weak vertical motions, in the presence of a decrease of moisture with height, generate the observed horizontal variations of moisture, although no objective support was offered in Mahrt (1991b).

These mesoscale transient disturbances ($\phi(x, t)^{*\prime}$) also occur for Flight 19 but are less coherent. We have also observed significant transient mesoscale disturbances in other data sets. Since the cause of such circulations is not known, we refer to them as "nameless mesoscale motions".

4. Mesoscale and Turbulent Fluxes

Some fraction of the fluxes at the aircraft level may be due to the direct transport by mesoscale motions (Betts *et al.*, 1990; Desjardins *et al.*, 1992). This fraction generally increases with height above the boundary layer. To provide a framework for the data analysis, the vertical flux of an arbitrary variable $\phi(x, t)$ is decomposed and averaged over a given subleg, in which case

$$[w\phi] = [w'\phi'] + [w'\phi^*] + [w^*\phi'] + w^*\phi^*\,, \tag{6}$$

where the operator [ ] again averages over individual sublegs and ϕ^* is the local average less the domain (flight leg) average. The first term on the right hand side is the turbulent flux, the last term is the direct flux due to "mesoscale" motions, here on the scale of 5 km. The two remaining cross-terms vanish identically for the present case of unweighted averaging.

The mesoscale flux is due to both the stationary component, partly related to

surface variability, and the transient part. These contributions are estimated by substituting decomposition (4) into (6) and averaging over all flight legs. We then obtain

$$\{[w\phi]\} = \{[w'\phi']\} + \{w^*\}\{\phi^*\} + \{w^{*\prime}\phi^{*\prime}\}\,, \tag{7}$$

where $\phi^{*\prime}$ is again the deviation of the instantaneous mesoscale (subleg average) value from the value averaged over all of the flight legs. The second term on the right hand side is the flux due to the stationary part of the mesoscale flow and the third term is the flux due to transient mesoscale motions. Since ($\{w^*\} = \{\phi^{*\prime}\} = 0$), the transient mesoscale flux will normally switch sign between flight legs and become small when averaged over the flight legs. We therefore also compute the average absolute value of the transient flux

$$\{\mathrm{abs}(w^{*\prime}\phi^{*\prime})\}\,. \tag{8}$$

This quantity is a measure of the typical instantaneous importance of the transient mesoscale flux.

Averaged over all flight legs, the mesoscale momentum flux $\{w^*v^*\}$ is on the order of 10% of the turbulent momentum flux as can be inferred from Figure 6 (solid bars). However, the average of the absolute value of the transient mesoscale momentum flux defined by Equation (8) (clear bars in Figure 6) is comparable to the value of the turbulent momentum flux (grey bars). Consequently, much of the mesoscale momentum flux is due to transient mesoscale disturbances and changes sign between aircraft legs.

The mesoscale fluxes $\{w^*\phi^*\}$ for heat (solid bars, Figure 6), carbon dioxide and ozone are generally small compared to the turbulence flux $\{[w'\phi']\}$ except where the turbulent flux becomes small. The weakness of the mesoscale fluxes is partly due to the fact that the vertical motion generated by the variation of surface temperature is weak at the 30 m level as discussed in Section 3. Only the upward mesoscale moisture flux (solid bars, Figure 6) appears to be significant, partly due to sinking dry air over nonirrigated areas. However, significant mesoscale moisture flux did not occur for flight 19. We conclude that mesoscale fluxes for these data are generally small.

5. Mesoscale Modulation of the Turbulent Momentum Flux

In order to study the relationship between spatially averaged fluxes and spatially averaged vertical gradients, it is necessary to examine the influence of mesoscale modulation of turbulent fluxes. This modulated turbulent flux is distinct from the direct mesoscale flux examined in the previous section.

Mesoscale modulation can lead to significant net modification of the spatially averaged flux as implied by the studies of Mahrt (1987), Claussen (1991) and Pinty (1991).

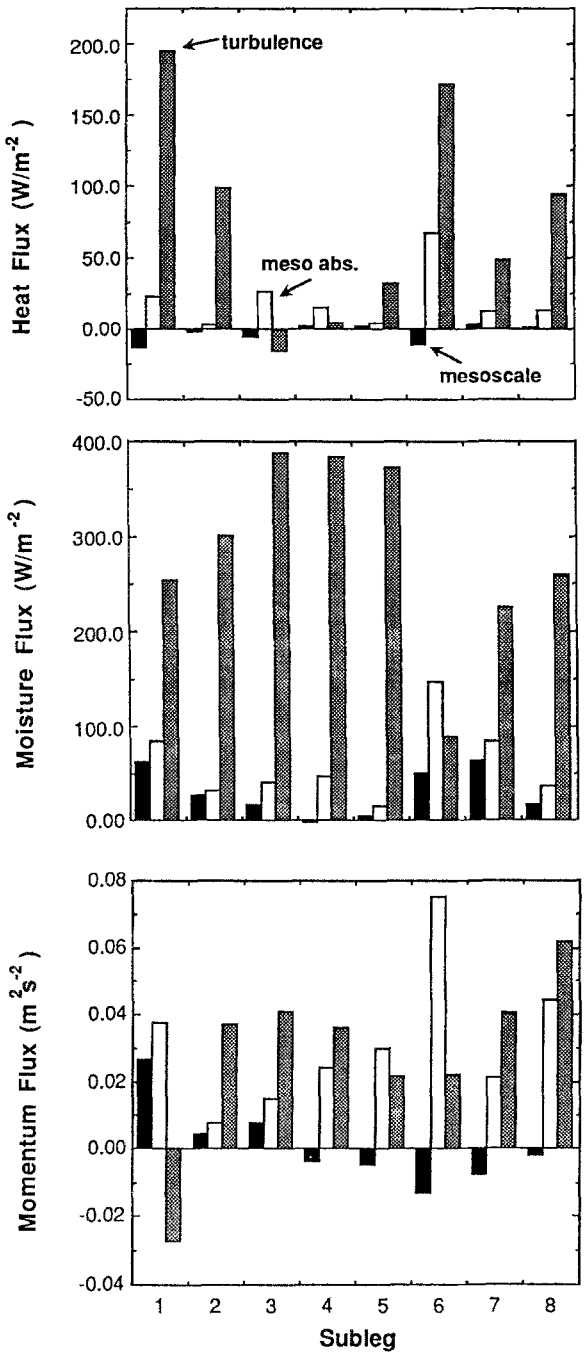

Fig. 6. The subleg average turbulent flux = $\{[w'\phi']\}$ (grey bars), mesoscale flux = $\{w^*\phi^*\}$ (solid bars) and average absolute value of the mesoscale flux = $\{\text{abs}(w^{*\prime}\phi^{*\prime})\}$ (clear bars) computed by averaging the fluxes over all of the flight legs for each subleg for heat, moisture and carbon dioxide for flight 13.

In this section, we examine momentum fluxes in terms of the following drag law:

$$[w'u'] = -[C_{Du}][V]^2 \operatorname{sign}[u]\,, \tag{9}$$
$$[w'v'] = [C_{Dv}][V]^2 \operatorname{sign}[v]\,,$$
$$[V] = ([u]^2 + [v]^2)^{1/2}\,,$$

where the drag coefficients for this approach are defined as:

$$C_{Du} = -[w'u']/[V]^2 \operatorname{sign}[u]\,, \tag{10}$$
$$C_{Dv} = -[w'v']/[V]^2 \operatorname{sign}[v]\,,$$

where again primes indicate turbulent fluctuations and the operator [ ] indicates local averaging over turbulent scales. With this approach, the direction of the stress is defined by C_{Du} and C_{Dv} so that the stress is allowed to be in a different direction than exactly opposite to the mean wind vector. This generalization accommodates the data analysis without any further assumption. The inclusion of the factors sign[u] and sign[v] defines the drag coefficients to be positive when the stress direction is opposite to the mean wind direction.

The magnitude of the stress is

$$([w'v']^2 + [w'u']^2)^{1/2} = C_D V^2\,,$$
$$C_D = (C_{Du^2} + C_{Dv^2})^{1/2}\,. \tag{11}$$

If the stress is exactly opposite to the wind direction, (9) reduces to the usual formulation

$$[w'u'] = -C_D V[u]\,,$$
$$[w'u'] = -C_D V[v]\,. \tag{12}$$

As defined in (1–2), we partition the flow into a domain average (such as an average along the aircraft leg), $\langle\phi\rangle$, the deviation of the local average (subleg or window average) from the domain average, ϕ^*, and the turbulent deviation (ϕ'). The drag coefficient is decomposed as

$$C_{Du} = [C_{Du}] = \langle C_{Du}\rangle + C_{Du^*}\,. \tag{13}$$

Then using the decomposition (1–2) for momentum and (13) for the drag coefficient, the turbulent momentum flux for the u-component can be expressed as

$$[w'u'] = -(\langle C_{Du}\rangle + C_{Du^*})(\langle V\rangle + V^*)^2 \operatorname{sign}[u]. \tag{14}$$

Averaging these fluxes over the entire domain, grouping terms and assuming Reynolds averaging such that $\langle u^*\rangle = 0$, we obtain an expression analogous to (13) in Claussen (1990)

$$-\langle[w'u']\rangle \operatorname{sign}[u] = \langle C_{Du}\rangle\langle V\rangle^2 + \langle C_{Du}\rangle\langle V^{*2}\rangle +$$
$$+ 2\langle V\rangle\langle C_{Du^*}V^*\rangle + \langle C_{Du^*}V^{*2}\rangle. \tag{15}$$

The expression for $\langle [w'v'] \rangle$ is exactly analogous to (15) and must be included to account for the total stress. Relationship (15) can easily be generalized for the case where the sign of the locally averaged wind components are changing with horizontal distance.

The first term on the right-hand side of (15) is the turbulent flux estimated in terms of the variables averaged over the spatial domain. These could be the grid area averaged variables resolved by a numerical model. The last three terms on the right-hand side are corrections due to modulation of the flow by the mesoscale motions and are not included in existing models. The second term on the right-hand side is the flux due to mesoscale variations of the wind speed, which always acts to increase the magnitude of the spatially averaged momentum flux. That is, the stress depends quadratically on the wind speed so that mesoscale increases of the wind speed act to increase the domain-averaged momentum flux more than mesoscale decreases of the wind speed act to decrease the flux.

The third and fourth terms on the right-hand side of (15) are due to mesoscale correlations between the wind and drag coefficient. Since the drag coefficient depends on stability, which in turn depends on wind speed, the mesoscale variations of the wind and the drag coefficient are correlated. For stable conditions, this correlation is positive, which acts to increase the spatially averaged flux. Conversely, this correlation is negative in the unstable case which acts to decrease the averaged flux. That is, the instability and drag coefficient are less in regions of strong wind speed which exceeds the effect of greater drag coefficient in regions of weak wind speed. The net effect is then to reduce the area-averaged momentum flux.

First consider the windy near-neutral case where C_{Du} is approximately constant (C_{Du^*} approximately zero). Then the third and fourth terms on the right hand side are small, in which case (15) becomes approximately

$$\langle [w'u'] \rangle \operatorname{sign}[u] = \langle C_{Du} \rangle \langle V \rangle^2 + \langle C_{Du} \rangle \langle V^{*2} \rangle . \tag{16}$$

For this case, the mesoscale modulation always acts to increase the domain-averaged momentum flux.

As the magnitude of the mean wind vector becomes small, the domain-averaged stress may become dominated by the second term on the right-hand side of (16) representing the contribution of mesoscale variations to the domain-averaged stress. When the domain-averaged wind vector vanishes, the domain-averaged momentum flux does not necessarily vanish, even though the direction of such a stress depends on the details of the subdomain variations.

To form the basis for future formulations in large-scale models, we can rewrite (15) in terms of an effective drag coefficient for the area-averaged momentum flux such that

$$-\langle [w'u'] \rangle \operatorname{sign}[u] = \langle C_{Du} \rangle_{\text{eff}} \langle V \rangle^2 , \tag{17}$$

where $\langle C_{Du} \rangle_{\text{eff}}$ absorbs the contribution of the extra Reynolds terms.

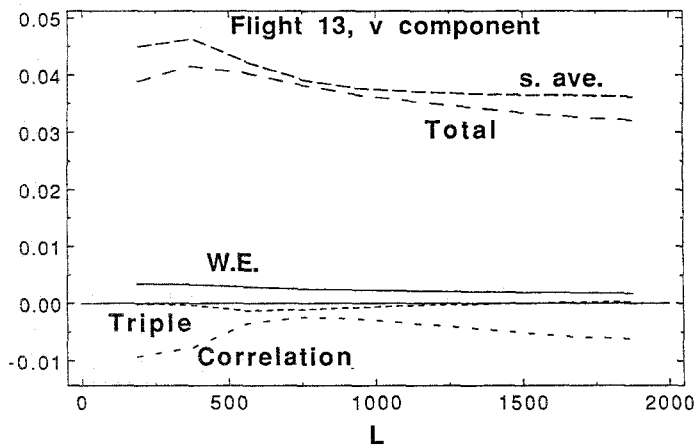

Fig. 7. The spatially averaged flux terms ($m^2 s^{-2}$) in (15) averaged over all of the flight legs as a function of scale. The terms are the actual momentum flux (total), the flux estimated in terms of spatially averaged variables (S. Ave.), the wind enhancement term (W.E.), the wind speed-drag coefficient correlation term (correlation) and the triple correlation term (triple).

6. Observed Mesoscale Modulation

The terms in (15) are now evaluated from the CODE data by defining the mesoscale flow to be a moving average over a window width of L'. We consider only the v-component since the flux for the u-component was weak. In the following, we evaluate the extra Reynolds flux terms (15) at the scale of maximum momentum flux, defined by a window width of 375 m (Figure 7) and then later briefly consider the extra Reynolds terms defined by the subleg averages (approximately 5 km scale). The 375 m window width is too small to be a formal division between turbulent and mesoscale motions; however, the dependence of the relative importance of the extra Reynolds terms on the window width is weak (Figure 7).

Averaging over all flight legs, the triple correlation term on the right hand side of (15) is a few percent or less of the total flux and therefore unimportant. The wind enhancement term acts to increase the stress by 5–10% (Figure 7). The decrease of the stress by the wind speed-drag coefficient correlation term is more important than the other extra Reynolds terms. At the scale of maximum flux, the wind speed – drag coefficient correlation term is about 25% of the spatially averaged momentum flux. This correlation term contributes to a net decrease of the spatially averaged stress (compared to use of area-averaged variables in the drag law). This net decrease is about 10–15% when averaged over all flights. The net decrease is 30–40% early in the afternoon but becomes negligible later when the surface heating becomes weak. This correlation term is related to differential heating over heterogeneous terrain. A sign shift is expected when the surface layer becomes stable. With stable conditions, the drag coefficient is enhanced where the wind speed increases so that the correlation term becomes positive.

This wind speed – drag coefficient correlation term for Flight 19 is the same order of magnitude as the momentum flux estimated in terms of spatially averaged variables, and the net momentum flux is an order of magnitude smaller than that estimated in terms of spatially averaged variables; however, the momentum fluxes are weak, less than $0.01\,m^2\,s^{-2}$. With sufficiently weak winds, the mesoscale variation of the wind is of comparable magnitude to the spatially averaged wind and the extra Reynolds terms in (15) are more likely to be important.

When the local averaging operator [ ] is defined as the subleg average instead of the moving average, the wind speed – drag coefficient correlation term is still the largest correction term but is reduced by a factor of two compared to the above estimates based on the moving average.

Significant reduction of the area-averaged momentum flux by the wind speed – drag coefficient correlation term is in qualitative agreement with modelling results of Claussen (1990) and indicates that (16) is a poor approximation for these data. The wind speed – drag coefficient correlation term results from the fact that the drag law with spatially averaged drag coefficient overestimates the flux in subgrid areas of strong wind speed. The stronger wind speed reduces the thermodynamic instability and therefore reduces the local drag coefficient. The total stress is still stronger in areas of strong wind speed but not as strong as would be predicted by a constant spatially averaged drag coefficient.

The above results indicate that the effective drag coefficient for application to the area averaged wind speed (17) can be significantly less than the area-averaged drag coefficient and that this reduction increases with surface heating and surface inhomogeneity and decreases with mean wind speed. With data from a wider variety of conditions, the reduction of the drag coefficient could be formulated most simply by modifying an existing similarity theory for the dependence of the drag coefficient on stability.

7. Heat Flux Decomposition

An analysis analogous to (15) has also been constructed for the heat flux using the difference of potential temperature between the 30 m aircraft level and the potential temperature at the ground surface based on the surface radiation temperature. We begin with the usual formulation for the surface turbulent heat flux

$$[w'\theta'] = C_H[V(z)]([\theta_{sfc}] - [\theta(z)]), \tag{18}$$

where C_H is the exchange coefficient for heat, $[V(z)]$ is the locally averaged wind speed and $[\theta(z)]$ is the locally averaged potential temperature at the observational level. The exchange coefficient C_H not only depends on stability and height above ground z but also depends on the way in which the surface temperature is measured. In practice, θ_{sfc} is the surface potential temperature corresponding to the surface radiation temperature or the temperature computed from a modelled surface energy budget. This choice of θ_{sfc} defines C_H.

Decomposing the flow according to (1–2) and decomposing the exchange coefficient for heat as in (13), substituting into (18) and averaging over the domain, the domain-averaged turbulent heat flux becomes

$$\langle [w'\theta'] \rangle = \langle C_H \rangle \langle V(z) \rangle \{ \langle \theta_{sfc} \rangle - \langle \theta(z) \rangle \} + \langle C_H \rangle \langle V(z)^* \{ \theta_{sfc^*} - \theta(z)^* \} \rangle + \\ + \langle C_{H^*} V(z)^* \{ \langle \theta_{fsc} \rangle - \langle \theta(z) \rangle \} + \langle V(z) \rangle \langle C_{H^*} \{ \theta_{sfc^*} - \theta(z)^* \} \rangle + \\ + \langle C_{H^*} V(z)^* \{ \theta_{sfc^*} - \theta(z)^* \rangle \, . \qquad (19)$$

The first term on the right hand side of (19) is the heat flux predicted in terms of domain-averaged variables. The second term is a correction term due to mesoscale correlation between the wind speed and vertical temperature difference while the third term is due to mesoscale correlation between the exchange coefficient and the wind speed. For the unstable case, the third term is expected to reduce the domain-averaged turbulent heat flux because the instability is normally less where the wind speed is stronger. Here, instability can be defined as $-z/L$, where L is the Obukhov length. The fourth term is due to the mesoscale correlation between the exchange coefficient and the vertical temperature gradient. This term acts to enhance the heat flux because the exchange coefficient is normally larger where the vertical temperature difference and instability are greater. The fifth term is a triple correlation term, which is expected to be small.

In applying the analysis to the CODE data, we discarded about 10% of the record over the upstream part of the irrigated area, where the vertical temperature difference and the sensible heat flux become quite small and are dominated by sampling errors. For the remainder of the CODE data, the correlation between the exchange coefficient and the vertical temperature difference is the the most important correction term, enhancing the domain-averaged heat flux by about 35%. The importance of this correlation term is due to the large spatial variation of surface temperature. As a result, the domain-averaged heat flux is larger than that predicted from domain-averaged variables. This contrasts with the results of Mahrt (1987) who found that the correlation between spatial variations of wind speed and the exchange coefficient was the dominant term leading to a decrease of the area-averaged heat flux. Pinty (1991) found that for moisture flux, the correlation between subgrid variations of wind speed and the exchange coefficient was also the dominant term leading to a decrease of the area-averaged moisture flux compared to that estimated from area-averaged variables. Both the studies of Mahrt and Pinty are based on mesoscale models of specific surface variability and use the same similarity formulation for the surface exchange coefficient. For most situations over land, the stability dependence of the exchange coefficient is more coupled to the vertical temperature difference than the vertical moisture difference, which would lead to the results of Pinty.

At the same time, the enhancement of the domain-averaged heat flux by the correlation term is constrained by the surface energy budget. The mathematical increase of the heat flux must be compensated by a reduction of surface evapor-

ation or modification of the other terms in the area-averaged surface energy budget. One could perform a partitioning and averaging analogous to (19) for all of the terms of the surface energy budget; however, surface specific humidity is difficult to assess. Specifying the surface specific humidity to be the saturation value allows evaluation of the potential evaporation, which then requires estimation of the soil water content and stomatal properties.

An effective exchange coefficient for the area-averaged heat flux can be defined in analogy to (17) such that

$$\langle w'\theta' \rangle = \langle C_H \rangle_{eff} \langle V(z) \rangle \{ \langle \theta_{sfc} \rangle - \langle \theta(z) \rangle \} , \tag{20}$$

where $\langle C_H \rangle_{eff}$ absorbs the correlation terms associated with spatial variability. The above results indicate that the effective exchange coefficient for heat is about 35% larger than the spatially averaged exchange coefficient.

8. Conclusions and Discussion

This study analyzed data from repeated low level aircraft runs over a heated surface with well defined variations of surface moisture and vegetation. The spatial and temporal variability of the surface heat flux into the atmosphere is almost completely described by the surface heterogeneity as is supported by a formal variance analysis. Spatial variations of surface fluxes of moisture and carbon dioxide are primarily influenced by the surface heterogeneity but also affected by transient mesoscale variations of unknown origin. In contrast, variation of momentum fluxes are significantly related to transient mesoscale circulations.

The area-averaged turbulent momentum flux is significantly less than that predicted from area-averaged variables because of a negative spatial correlation (mesoscale modulation) between the drag coefficient and the wind speed within the averaging domain. In the stably stratified boundary layer, this "extra" Reynolds term reverses sign and enhances the area-averaged momentum flux. For the unstable case, positive correlation between the exchange coefficient for heat and the air-surface temperature difference within the averaging area enhances the area-averaged heat flux beyond what would be predicted by existing similarity formulations. This enhancement is largely due to the mesoscale surface variability and is therefore expected to vary with different geographical situations.

For the present data, the direct mesoscale momentum flux is of opposite sign to the turbulence flux and therefore also reduces the area-averaged momentum flux. However, direct mesoscale transport is less important than the extra Reynolds term resulting from the above mesoscale spatial modulation of the turbulent momentum flux. In fact, mesoscale transport of all of the quantities is generally small for the data analyzed here. Apparently the horizontal scale of the surface variability is too small to generate significant mesoscale vertical motions at low levels.

Formulation of the subgrid fluxes must recognize that transport of momentum

is quite different from that of heat, moisture and carbon dioxide. In the present study, the turbulent momentum flux is significantly modified by transient mesoscale motions while the vertical fluxes of heat, moisture and carbon dioxide are more related to the surface variability.

Acknowledgments

We are especially indebted to James Pederson who organized and administered the CODE project and provided some of the support data for this study. The computational assistance of Michael Ek and Wayne Gibson and the useful comments of Martin Claussen and the reviewer are gratefully acknowledged. This material is based upon work supported by Grant DAA H04–93–G-0019 from the Army Research Office and grant ATM-8912736 from the Physical Meteorology Program of the National Sciences Foundation. The field program was sponsored by California Air Resources Board. Funding for the Twin Otter research aircraft was provided by the San Joaquin Valley Air Pollution Study Agency, in collaboration with the Pacific Gas and Electric Company, The Electric Power Research Institute and the California Air Resources Board, and by the National Research Council of Canada.

References

André, J. C., Bougeault, P., Mafouf, J.-F., Mascart, P., Noilhan, J. and Pinty, J.-P.: 1989, 'Impact of Forests on Mesoscale Meteorology', *Phil. Trans. R. Soc. Lond.* **B324**, 407–422.

Avissar, R. and Pielke, R. A.: 1989, 'A Parameterization of Heterogeneous Land Surfaces for Atmospheric Numerical Models and its Impact on Regional Meteorology', *Mon. Wea. Rev.* **117**, 2113–2136.

Bache, D. H. and Unsworth, M. H.: 1977, 'Some Aerodynamic Features of a Cotton Canopy', *Quart. J. Roy. Meteorol. Soc.* **103**, 121–134.

Betts, A. K., Desjardins, R. L., Macpherson, J. I. and Kelly, R. D.: 1990, 'Boundary-Layer Heat and Moisture Budgets from FIFE', *Boundary-Layer Meteorol.* **50**, 109–138.

Claussen, M.: 1990, 'Area-averaging of Surface Fluxes in a Neutrally Stratified, Horizontally Inhomogeneous Atmospheric Boundary Layer', *Atmos. Envir.* **24a**, 1349–1360.

Claussen, M.: 1991, 'Estimation of Areally-averaged Surface Fluxes', *Boundary-Layer Meteorol.*, **54**, 387–410.

de Bruin, H. A. R., Bink, N. J. and Kroon, L. J. M.: 1991, 'Fluxes in the Surface Layer under Advective Conditions', in T. J. Schmugge and J.-C. André (eds.), *Land Surface Evaporation; Measurement and Parameterization*, pp. 157–170, Springer Verlag.

Desjardins, R. L., MacPherson, J. I., Schuepp, P. H., and Hayhoe, H.: 1992, 'Airborne Flux Measurements of CO_2, sensible and latent heat over the Hudson Bay Lowland', *J. Geophys. Res.*,

Doran, J. C. and Colleagues.: 1992, 'The Boardman Regional Flux Experiment', *Bull. Amer. Meteorol. Soc.* **73**, 1785–1795.

Ducoudré, N. I., Laval, K. and Perrier, A.: 1993, 'SECHIBA, a New Set of Parameterizations of the Hydrologic Exchanges at the Land/Atmosphere Interface within the LMD Atmospheric General Circulation Model', *J. of Clim.* **6**, 248–273.

Gamage, N., and Hagelberg, C.: 1993, 'Detection and Analysis of Microfronts and Associated Coherent Events Using Localized Transforms', *J. Atmos. Sci.* **50**, 750–756.

Garratt, J. R.: 1990, 'The Internal Boundary Layer – a Review', *Boundary-Layer Meteorol.* **50**, 171–203.

Garratt, J. R.: 1992, *The Atmospheric Boundary Layer*, Cambridge University Press. 316 pp.

Hadfield, M. G., Cotton,W. R. and Pielke, R. A.: 1992, 'Large-eddy Simulations of Thermally Forced Circulations in the Convective Boundary Layer. Part II: The Effect of Changes in Wavelength and Wind Speed', *Boundary-Layer Meteorol.* **58**, 307–327.

Hechtel, L. M., Moeng, C.-H. and Stull, R. B.: 1990, 'The Effects of Nonhomogeneous Surface Fluxes on the Convective Boundary Layer: A Case Study Using Large-eddy Simulation', *J. Atmos. Sci.* **47**, 1721–1741.

Huang, X. and Lyons, T. J.: 1993, 'A Simple Land Surface Atmosphere Model', *Aust. Meteorol. Mag.*, submitted.

Lange, A. R. G., McNaughton, K. G., Chen, F., Bradley, E. F. and Ohtaki, E.: 1983, 'Inequality of Eddy Transfer Coefficients for Vertical Transport of Sensible and Latent Heats During Advective Inversions', *Boundary-Layer Meteorol.* **25**, 25–41.

MacPherson, J. I.: 1992, 'NRC Twin Otter Operations in the 1991 California Ozone Deposition Experiment', Rept LTR-FR-118. Flight Research Laboratory, National Research Council., Ottawa, Canada K1A 0R6.

MacPherson, J. I., Schmidt, R. W. H., Jochum, A. M., Pearson, R. Jr., Neumann, H. H. and Den Hartog, G.: 1993, 'Ozone Flux Measurement on the NRC Twin Otter during the 1991 California Ozone Deposition Experiment', *Proceedings of the American Meteorological Society Eighth Symposium on Meteorological Observations*. Anaheim, CA.

Mahrt, L.: 1987, 'Grid-averaged Surface Fluxes', *Mon. Wea. Rev.* **115**, 1550–1560.

Mahrt, L.: 1991a, 'Eddy Asymmetry in the Sheared Heated Boundary Layer', *J. Atmos. Sci.* **48**, 472–492.

Mahrt, L.: 1991b, 'Boundary-layer Moisture Regimes', *Quart. J. Roy. Meteorol. Soc.* **117**, 151–176.

Mason, P. J.: 1988, 'The Formation of Areally-averaged Roughness Lengths', *Quart. J. Roy. Meteorol. Soc.* **114**, 399–420.

Pielke, R. A. and Avissar, R.: 1990, 'Influence of Landscape Structure on Local and Regional Climate', *Landscape Ecology* **4**, 133–155.

Pinty, J.-P.: 1991, 'A Numerical Study of Surface Flux Variability with a Mesoscale Model: Application to the HAPEX-MOBILHY Experiment', *The 10th Conference on Biomet. and Aerobio.* Amer. Meteorol. Soc. 181–184.

Segal, M., Schreiber, W. E., Kallos, G., Garrat, J. R., Rodi, A., Weaver, J. and Pielke, R. A.: 1989, 'The Impact of Crop Areas in Northeast Colorado on Midsummer Mesoscale Thermal Circulations', *Mon. Wea. Rev.* **117**, 809–825.

Segal, M. and Arritt, R. W.: 1992, 'Non-classical Mesoscale Circulations Caused by Surface Sensible Heat Flux Gradients', *Bull. Amer. Meteorol. Soc.* **73**, 1593–1604.

Smith, E. A., Hsu, A. Y., Crosson, W. L., Field, R. T., Fritschen, L. J., Gurney, R. J., Kanemasu, E. T., Kustas, W. P., Nie, D., Shuttleworth, W. J., Stewart, J. B., Verma, S. B., Weaver, H. L. and Wesely, M. L.: 1992, 'Area-averaged Surface Fluxes and Their Time-space Variability over the FIFE Experimental Domain', *J. Geophys. Res.* **97**, 18599–18622.

Smith, B. and Mahrt, L.: 1981, 'A Study of Boundary-Layer Pressure Adjustments', *J. Atmos. Sci.* **38**, 334–346.

Vugts, H. F. and Businger, J. A.: 1977, 'Air Modification Due to a Step Change in Surface Temperature', *Boundary-Layer Meteorol.* **11**, 295–306.